Adaptive resolution scheme for efficient hybrid atomistic-mesoscale molecular dynamics simulations of dense liquids

Matej Praprotnik,* Luigi Delle Site, and Kurt Kremer
Max-Planck-Institut für Polymerforschung, Ackermannweg 10, D-55128 Mainz, Germany
(Received 22 February 2006; published 2 June 2006)

The adaptive resolution scheme (AdResS) for efficient hybrid particle-based atomistic/mesoscale molecular dynamics (MD) simulations recently introduced by us, [J. Chem. Phys. **123**, 224106 (2005)] is extended to high density molecular liquids with spherical boundaries between the atomistic and mesoscale regions. The key feature of this approach is that it allows for a dynamical change of the number of molecular degrees of freedom during the course of a MD simulation by an on-the-fly switching between the atomistic and mesoscopic levels of detail. Pressure and density variations occurring at the atomistic/mesoscale boundary in the original version are considerably reduced employing the improved methodology presented here.

DOI: 10.1103/PhysRevE.73.066701 PACS number(s): 02.70.Ns, 61.20.Ja, 61.25.Em

I. INTRODUCTION

Molecular liquids and soft matter are typical examples, where the interplay between different length scales determines the relevant properties of the system. The theoretical study of such systems using computer simulation techniques, which aim for a comprehensive understanding, therefore, requires a multiscale modeling approach to bridge between the various length and time scales involved. In order to efficiently address these problems we have recently introduced the adaptive resolution scheme (AdResS) for hybrid particle-based atomistic/mesoscale molecular dynamics (MD) simulations [1], which combines the merits of fully atomistic with those of the mesoscopic MD simulations. The unique feature that separates our new approach from other scale bridging particle-based simulations [2–6] is that it allows us to change the level of detail and hence the number of molecular degrees of freedom in the system on-the-fly during the course of the MD simulation. Particles and/or molecules can move freely from one resolution regime into the other. By such a dynamical switching between the atomistic and mesoscopic resolutions one has the option to treat only as many degrees of freedom as absolutely necessary for the problem considered. This approach is thus suited for molecular systems, where spatially localized domains with the required atomistic resolution exchange particles with the remainder of the system sufficiently described on the mesoscopic level of detail. For example, one could run a system on a mesoscale level and then, depending on some chosen criteria, zoom into some subdomain of the system, where a more detailed resolution would be required at a given instant. The applicability of the method is by no means limited to solely couple the atomistic and mesoscopic levels of detail but can also be employed to link two arbitrary mesoscopic domains with different levels of coarse graining. Extensions in this direction where more than two levels of resolution are treated are, in principle, straightforward in this context. Recently, a similar idea was followed within a Monte Carlo simulation [7]. Both schemes give the same molecular densities in both regimes. We here, however, especially focus on the molecular structure, which is not given in Ref. [7].

In Ref. [1] we have tested the method on the medium dense model liquid of model tetrahedral molecules where the atomistic region was separated from the coarse-grained domain by a flat boundary. This is the geometry one would apply, for example, in studies of liquids near (metal) surfaces [2–4,8,9], where close to the surface the detailed structure of the liquid is crucial, while farther away a more coarse-grained model is fully sufficient. For the case of a synthetic or biological macromolecule embedded in a solvent, see for example, Ref. [6], a spherical geometry is more appropriate with a spherically shaped atomistic region surrounded by a coarse-grained domain. Thus the first goal of this paper is to generalize the method from Ref. [1] to be also applicable for these kind of situations.

One can consider the resolution switching as a geometry induced first-order phase transition. Therefore, at equilibrium, boundary conditions analogous to two phase coexistence must hold implying that the chemical potentials, pressures, and temperatures in both regions with different levels of detail are the same. These conditions assure that there is no net flux of molecules between the two regions, which guarantees that the liquid is homogeneous across the simulation box as it is in the reference all-atom system. We demonstrated in Ref. [1] that when using our method any spurious unphysical net flux, resulting in a density difference between the two regimes, is avoided. We show in the present study that small ($\sigma \approx 5\%$) pressure and density variations in the transition layer between the atomistic and coarse-grained regimes emerging as an artifact of the original scheme [1] can be reduced by a careful reparametrization of the effective pair potential in the transition layer.

We have also extended the method from medium to high (or regular) density liquids, where a tabulated effective pair potential must be used instead of the analytical one to correctly reproduce the equation of state of the reference all-atom system around the considered phase point [10].

*On leave from the National Institute of Chemistry, Hajdrihova 19, SI-1001 Ljubljana, Slovenia. Electronic mail: praprot@cmm.ki.si

II. ALL-ATOM MODEL LIQUID

To test and validate the new approach to multiscale MD simulations we resort to the generic explicit (*ex*) model of a liquid of tetrahedral molecules as introduced in Ref. [1]. This model system mimics a typical soft matter system, e.g., a colloidal sphere system, liquid methane, etc. Each molecule in this model is composed of four equal atoms with mass m_0. Their size σ is fixed via the repulsive Weeks-Chandler-Andersen potential

$$U_{rep}^{atom}(r_{i\alpha j\beta}) = \begin{cases} 4\varepsilon\left[\left(\frac{\sigma}{r_{i\alpha j\beta}}\right)^{12} - \left(\frac{\sigma}{r_{i\alpha j\beta}}\right)^{6} + \frac{1}{4}\right]; & r_{i\alpha j\beta} \leqslant 2^{1/6}\sigma \\ 0; & r_{i\alpha j\beta} > 2^{1/6}\sigma \end{cases} \tag{1}$$

with the cutoff at $2^{1/6}\sigma$. We use σ as a unit of length and ε as a unit of energy. Here $r_{i\alpha j\beta}$ is the distance between the atom i of the molecule α and the atom j of the molecule β. The neighboring atoms in a given molecule α are connected by the finite extensible nonlinear elastic (FENE) bonds

$$U_{bond}^{atom}(r_{i\alpha j\alpha}) = \begin{cases} -\frac{1}{2}kR_0^2 \ln\left[1 - \left(\frac{r_{i\alpha j\alpha}}{R_0}\right)^2\right]; & r_{i\alpha j\alpha} \leqslant R_0 (3) \\ \infty; & r_{i\alpha j\alpha} > R_0 \end{cases} \tag{2}$$

with divergence length $R_0 = 1.5\sigma$ and stiffness $k = 30\varepsilon/\sigma^2$.

III. COMPUTATIONAL METHOD

A. Adaptive resolution MD scheme (AdResS)

Our recently introduced AdResS [1] consists of two main steps. First, we map the fully atomistic *ex* model to a coarse-grained (*cg*) mesoscopic model (in this specific case composed of a one-particle coarse-grained molecule with mass $4m_0$) and derive the effective pair potential $U^{cm}(r)$ between coarse-grained molecules. We derive the effective *cg* potential in such a way that the center-of-mass radial distribution function (RDF_{cm}) and pressure of the *cg* system match the corresponding RDF_{cm} and pressure of the *ex* system at a given density and temperature [11]. For the effective pair potential derivation one can resort to various methods found in the literature, see, e.g., Refs. [10,12–14]. In order to avoid any density difference and net flux between the two regimes, the *cg* potentials have to be chosen such that the equations of state for the *ex* and *cg* systems coincide around the state point considered.

Second, we introduce the hybrid atomistic-mesoscopic (*ex-cg*) model system composed of explicit and coarse-grained molecules as presented in the Figs. 1(a) and 1(b). In the present study, the atomistic region, which is positioned at the center of the simulation box, has a spherical shape. It is surrounded by the coarse-grained domain, which is spread over the rest of the system with standard periodic boundary conditions. The two regions freely exchange molecules through a transition regime, where they change their resolution and their number of degrees of freedom accordingly as described in Ref. [1]. This interface region contains hybrid molecules, each of which is composed of the explicit atomistically resolved molecule with an additional massless center-of-mass particle serving as an interaction site. This transition, which has to be smooth for MD simulations, is governed by a weighting function $w(r)$. The latter smoothly interpolates between the two regimes. For the present spherical geometry we adapt the function used before [1] for the case of the flat boundary, in the following functional form:

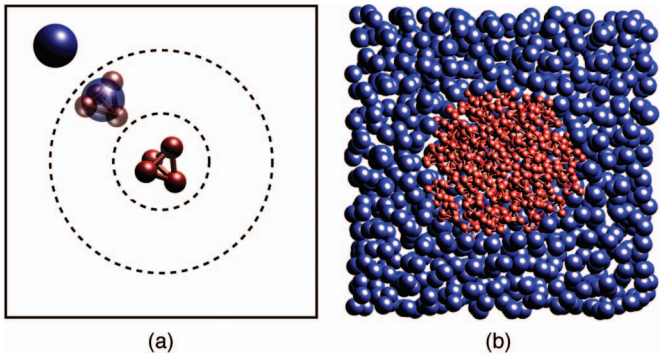

FIG. 1. (Color) (a) Schematic representation of the hybrid system with spherically shaped regions modeled with different levels of detail. In the center there is the all-atom regime with the tetrahedral molecules surrounded by the transition regime with the hybrid molecules followed by the mesoscopic regime with one-particle coarse-grained molecules. (b) Cross section of the hybrid system with spherical resolution boundaries at molecular number density $\rho = 0.175/\sigma^3 \approx 1.0/\sigma_{cg}^3$ and $T = 1.0\varepsilon/k_B$, where σ_{cg} is the excluded volume diameter of the coarse-grained molecule and k_B the Boltzmann's constant. For the presentation convenience the transition regime is not shown.

$$w(r) = \begin{cases} 1; & r_0 > r \geqslant 0 \\ 0; & r \geqslant r_0 + d \\ \cos^2\left[\frac{\pi}{2d}(r - r_0)\right]; & r_0 + d > r \geqslant r_0 \end{cases} \tag{3}$$

where r_0 is the radius of the atomistic region and d the interface region width (see Fig. 2).

With this transition function, we couple the atomic and mesoscopic length scales via the ansatz for the total intermolecular force acting between the centers of mass of molecules α and β, as given below for the spherical geometry:

$$\mathbf{F}_{\alpha\beta} = w(R_\alpha)w(R_\beta)\mathbf{F}_{\alpha\beta}^{atom} + [1 - w(R_\alpha)w(R_\beta)]\mathbf{F}_{\alpha\beta}^{cm}, \tag{4}$$

where

$$\mathbf{F}_{\alpha\beta}^{cm} = -\frac{\partial U^{cm}}{\partial \mathbf{R}_{\alpha\beta}}. \tag{5}$$

The force

$$\mathbf{F}_{\alpha\beta}^{atom} = \sum_{i\alpha, j\beta} \mathbf{F}_{i\alpha j\beta}^{atom} \tag{6}$$

is the sum of all pair atom interactions between explicit atoms of the molecule α and explicit atoms of the molecule β

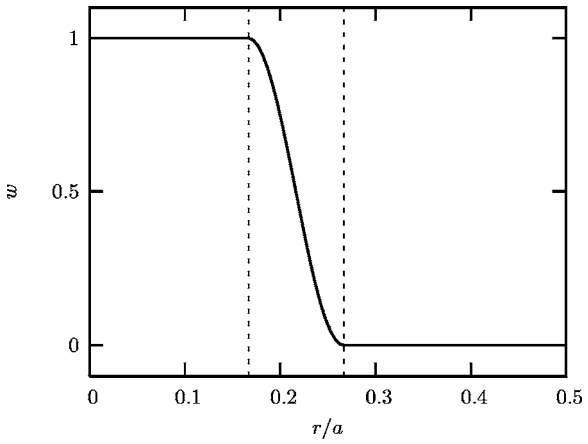

FIG. 2. The weighting function $w(r) \in [0,1]$ defined by Eq. (7). The values $w=1$ and $w=0$ correspond to the atomistic and coarse-grained regions of the hybrid atomistic-mesoscopic system with the box length a, respectively, whereas the values $0<w<1$ correspond to the interface layer. Shown is the example where the width d of the interface layer is $a/10$ and the radius of the atomistic region r_0 is $a/6$. The vertical lines denote the boundaries of the interface layer.

$$\mathbf{F}_{i\alpha j\beta}^{atom} = -\frac{\partial U^{atom}}{\partial \mathbf{r}_{i\alpha j\beta}}. \tag{7}$$

The vector $\mathbf{r}_{i\alpha j\beta}=\mathbf{r}_{i\alpha}-\mathbf{r}_{j\beta}$ is the relative position vector of atoms $i\alpha$ and $j\beta$, $\mathbf{R}_{\alpha\beta}=\mathbf{R}_{\alpha}-\mathbf{R}_{\beta}$ is the relative position vector of the centers of mass of the molecules α and β, R_α and R_β are the center-of-mass distances of the molecules α and β from the center of the simulation box, respectively. The weighting function $w \in [0,1]$ is defined in such a way that values $0<w<1$ correspond to a hybrid molecule with extreme cases $w=1$ and $w=0$ corresponding to a four-atom tetrahedral molecule and one-particle coarse-grained molecule, respectively. When crossing the boundaries between different regimes molecules retain their linear momentum and gain or loose (depending on if they leave or enter the coarse-grained regime) the equilibrated vibrational and rotational degrees of freedom [1,15–19]. Note that by this choice of interactions in the transition regime, the hybrid molecule interacts with molecules in the mesoscale regime on a mesoscale-mesoscale level. In contrast, the interactions of the hybrid molecules with the molecules in the explicit regime are a combination of the explicit-explicit and mesoscopic-mesoscopic interactions in order to smoothly and efficiently equilibrate additional degrees of freedom upon moving into the explicit regime [20].

The switching of the resolution can be viewed as the geometrically induced first-order phase transition with the weighting function w playing the role of an order parameter. Exploiting this analogy the rotational and vibrational parts of the molecules' free energy can be considered as the latent heat at this "resolution transition." Therefore, this method must be employed together with a thermostat, which couples locally to the particle motion [1] and provides a mean to deliver or absorb the related "latent heat."

As demonstrated in Ref. [1] for the case of the flat boundary between regions with different levels of detail using the method described above, at equilibrium, the boundary conditions similar to the two phase coexistence

$$\mu_{ex}=\mu_{cg}, \quad p_{ex}=p_{cg}, \quad T_{ex}=T_{cg}, \tag{8}$$

are implicitly satisfied. Here μ_{ex}, p_{ex}, T_{ex} and μ_{cg}, p_{cg}, T_{cg} are the chemical potentials, pressures, and temperatures of the liquid in the atomistic and coarse-grained domains, respectively. The conditions (8) guarantee that there is no net flux of molecules between the atomistic and coarse-grained regions.

IV. MULTISCALE SIMULATION PROTOCOL

We carried out our hybrid multiscale simulations using the ESPResSo package [21], developed at our institute. We employed the replacement hybrid model system [1] and performed MD simulations with the Langevin thermostat integrating the Langevin equation

$$m_i \frac{d^2\mathbf{r}_i}{dt^2} = \mathbf{F}_i - m_i\Gamma\frac{d\mathbf{r}_i}{dt} + \mathbf{W}_i(t), \tag{9}$$

for each particle in the system, where m_i is the mass of the particle i, $\mathbf{F}_i$ is the total force acting on the respective particle, Γ is a friction constant, and $\mathbf{W}_i$ is the random force of a heat bath [22]. The value of the friction constant is $\Gamma=0.5\tau^{-1}$, where $\tau=(\varepsilon/m_0\sigma^2)^{-1/2}$. We sample the random force from a uniform distribution [23]. Periodic boundary conditions and the minimum image convention [24] are employed. For the integration a standard velocity Verlet algorithm with a $\Delta t=0.005\tau$ time step was used. After warm-up and equilibration, trajectories of 7500τ were obtained, with configurations stored every 5τ time for analysis. This production runs are performed with a $10^9\varepsilon/\sigma$ force capping to prevent possible force singularities that could emerge due to overlaps with the neighboring molecules when a given molecule enters the interface layer from the coarse-grained side [1].

All MD simulations are performed at temperature $T=\varepsilon/k_B$ and two molecular number densities $\rho=n/V=0.1/\sigma^3$ and $0.175/\sigma^3$, with n being the number of molecules. In both cases $n=5000$, corresponding to a cubic box size of $a=36.845\sigma$ or 30.57σ for the low and the high density, respectively. The molecules can be either the explicit, coarse-grained or hybrid. In the case of the all-atom system these molecular densities correspond to $\varrho=N/V=0.4/\sigma^3$ and $0.7/\sigma^3$ particle number densities, respectively, with N being the number of particles. To compare our model system densities with the Lennard-Jones liquid densities we use the same estimate for the excluded volume diameter of the coarse-grained molecule σ_{cg} as in Ref. [1], i.e., the distance, where the repulsive effective pair potential between the coarse-grained molecules in our simulations equals k_BT ($\sigma_{cg}\approx 1.7\sigma$ and $\sigma_{cg}\approx 1.795\sigma$ for the medium and high density liquids, respectively). The molecular number density $\rho=0.1/\sigma^3\approx 0.5/\sigma_{cg}^3$ then corresponds to a medium dense liquid while the higher density $\rho=0.175/\sigma^3$

$=0.175(\sigma_{cg}/\sigma)^3/\sigma_{cg}^3 \approx 1.0/\sigma_{cg}^3$ corresponds to a typical high density Lennard-Jones liquid. The reduced Lennard-Jones units [24] are used throughout.

To treat all "types" of molecules on the equal basis, we define the temperature and pressure according to the lower level of detail, i.e., we use the translational temperature [24] and molecular pressure [25,26] for the definitions of temperature and pressure in the system [1].

V. RESULTS AND DISCUSSION

A. Mapping of the coarse-grained to the all-atom model

1. Medium dense liquid

We define the effective interactions between the coarse-grained molecules in the system at $\rho=0.1$ and $T=1$ using the effective pair potential U^{cm} derived in Ref. [1]. This is parametrized with the analytical Morse potential

$$U^{cm}(r) = \gamma\{1-\exp[-\kappa(r-r_c)]\}^2 \tag{10}$$

with parameters $\gamma=0.105$, $\kappa=2.4$, $r_c=2.31$, and cutoff at r_c. The effective potential given by Eq. (10) is determined in such a way that the *cg* system reproduces the structure and the pressure of the reference *ex* system at the corresponding state point.

Our coarse-graining procedure does not incorporate the information about the energy fluctuations in the system. To compare the latter for the *ex* and *cg* systems we calculated the heat capacity of the respective systems formally defined as

$$C_V = \left(\frac{\partial U}{\partial T}\right)_V = \frac{\langle (E-\langle E\rangle)^2\rangle}{T^2} \tag{11}$$

where $U=\langle E\rangle$ and E are the internal and total energies of the system, respectively. The brackets $\langle\ \rangle$ denote the time average. The values of the heat capacities per molecule are $C_V^{ex}=9.4\pm0.3$ and $C_V^{cg}=2.0\pm0.1$ for the *ex* and *cg* systems, respectively. Their ratio $C_V^{ex}/C_V^{cg}=4.7$, close to 4. In general, the heat capacity is proportional to the number of degrees of freedom in the system. This number is 4 times higher in the *ex* than in the *cg* system (an explicit molecule has 3 translational, 3 rotational, and 6 vibrational degrees of freedom compared to only 3 translational degrees of freedom of a coarse-grained molecule). For the noninteracting molecules the ratio C_V^{ex}/C_V^{cg} would therefore be exactly 4. This is not the case for the liquid due to the contribution of the intermolecular interaction potential to the internal energy of the liquid. We have also computed the respective C_Vs using a smaller time step $\Delta t=0.0025$ and/or smaller friction constant $\Gamma=0.25$ and obtained similar values (within the computational error) indicating that our simulation protocol is correct.

2. High density liquid

A general feature of the effective pair potentials is that they are density and temperature dependent [27]. Therefore, one can reproduce the equation of state of a given all-atom system only at a certain range around the state point of interest by using an appropriate coarse-grained model with a chosen effective pair potential. In the study presented in Ref. [1] we were able to reproduce the equation of state of the *ex* system at $T=1$ and densities up to $\rho=0.125$ exploiting the *cg* model with the analytical effective pair potential given by Eq. (10). To also reproduce the respective equation of state, i.e., the structure and pressure of the *ex* system, at a high density of $\rho=0.175$ that corresponds to a dense Lennard-Jones liquid we have to resort to tabulated numerical potential.

We derive the effective pair potential using the iterative Boltzmann inversion [12]. We use the potential given by Eq. (10) as the initial guess $U_{tab_0}^{cm}(r)$ for the effective pair potential of the *cg* system at $\rho=0.175$ and $T=1$. This potential is then further optimized via the iterative procedure

$$U_{tab_{k+1}}^{cm}(r) = U_{\mathrm{tab}_k}^{cm}(r) + T\ln\frac{g_k^{cm}(r)}{g_{ex}^{cm}(r)}, \tag{12}$$

where $U_{tab_k}^{cm}(r)$ and $g_k^{cm}(r)$ are the effective pair potential and corresponding RDF_{cm} at the kth iteration.

In order to also match the pressure of the respective model system we add a linear correction term

$$\Delta U^{cm}(r) = U_0\left(1-\frac{r}{r_c}\right), \tag{13}$$

which vanishes at $\Delta U^{cm}(r_c)=0$ and has $U_0=\Delta U^{cm}(r=0)$ as the only parameter [10]. By the correction given by Eq. (13) we add a weak constant force to the effective force in such a way that that the total effective force and potential are zero at the cutoff r_c. The latter is set to 3.5 to match the RDF_{cm}s up to the second maximum. Depending on the pressure in the current iteration being above or below the target value of the reference *ex* system, U_0 is negative or positive. The pressure correction Eq. (13) acts mostly on the long-range part of the pair interactions. In contrast, the structure of the system is almost completely determined by the short-range part of the pair interactions [28].

In Fig. 3(a) we present the tabulated numerical effective pair potential $U_{tab}^{cm}(r)$ obtained after 5 iterations with $U_0=0.2$ followed by another 5 iterations with $U_0=0.1$. The RDF_{tab}s and tabulated potential $U_{tab}^{cm}(r)$ are calculated with $\Delta r=0.01$. Between these points we use a linear interpolation for the potential and force evaluation. For the RDF_{cm}s calculation we use the centers of mass of all the molecules in the simulation box.

The tabulated numerical effective pair potential $U_{tab}^{cm}(r)$ for $\rho=0.175$ is softer than the corresponding effective pair potential given by Eq. (10) as can be noticed from Fig. 3(a). It also exhibits a very shallow negative minimum despite the fact that all the interactions in the all-atom system are purely repulsive. This many-body effect here arises from the pressure correction defined by Eq. (13).

In Fig. 3(b) are depicted RDF_{cm}s of the *ex* and *cg* systems at $\rho=0.175$ and $T=1$. Although due to facilitated molecular rotations in our model liquid the height of the first maximum in the RDF_{cm} of the *ex* system is lower as in typical highly dense liquids the number of nearest neighbors up to the first minimum at $r=2.625$ is 12.83, a typical number for a highly

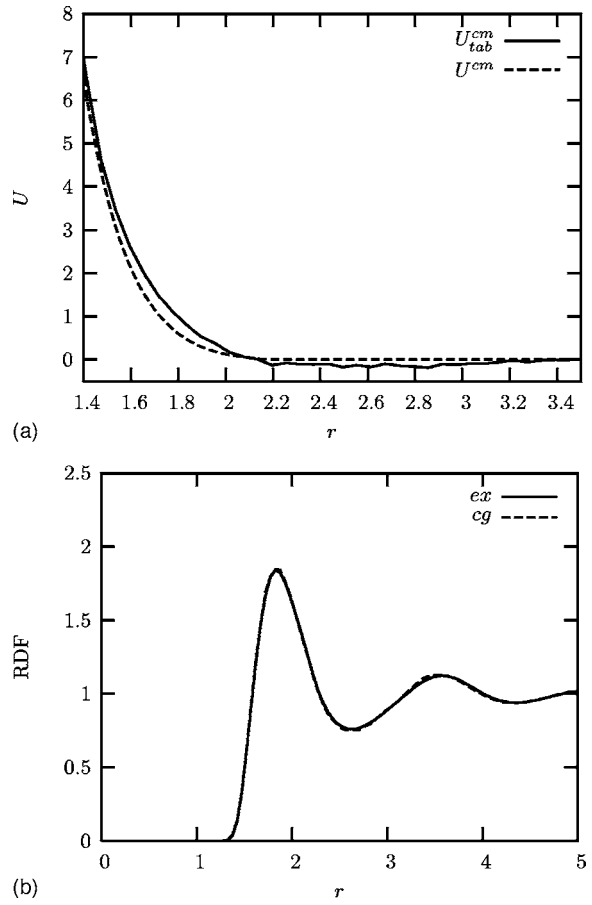

FIG. 3. (a) The tabulated effective potential $U_{tab}^{cm}(r)$ for the *cg* system at $\rho=0.175$ and $T=1$. Shown is also $U^{cm}(r)$, which holds for $\rho=0.1$ as given by Eq. (10) for comparison. (b) RDF_{cm}s of the *ex* and *cg* systems at $\rho=0.175$ and $T=1$. The RDF_{cm}s match to the line-thickness.

correlated liquid. This shows that the density of our model liquid indeed corresponds to a highly dense Lennard-Jones liquid. The RDF_{cm} of the *cg* system using the $U_{tab}^{cm}(r)$ for defining the effective interactions in the system matches to within line thickness with the reference RDF_{cm} of the *ex* system.

As a merit function of the evaluated RDF_{cm}s we introduce the penalty function f_p defined as

$$f_p = \int [g^{cm}(r) - g_{ex}^{cm}(r)]^2 \exp(-r)dr, \qquad (14)$$

where g_{ex}^{cm}, which is taken as a reference, is the RDF_{cm} of the *ex* system [1,12]. The RDF_{cm}s are calculated in the range $r \in [0,5]$ with $\Delta r=0.05$.

TABLE I. Penalty function f_p defined by Eq. (14) and average pressure for *ex* and *cg* systems at $\rho=0.175$ and $T=1$.

System	$f_p \times 10^3$	p
ex	0	1.99±0.02
cg	0.0262	1.98±0.02

TABLE II. Penalty function f_p defined by Eq. (14) and the average pressure p for *ex*-*cg* systems at $\rho=0.1$ and $T=1$ as a function of r_0. 0^{ex} and 0^{cg} denote the *ex* and *cg* systems, respectively. The corresponding values of f_p and p are taken from Ref. [1].

r_0	$f_p \times 10^3$	p
0^{ex}	0	0.379±0.009
0^{cg}	0.2067	0.378±0.004
6.0	0.2020	0.379±0.003
7.0	0.1961	0.379±0.002
8.0	0.1925	0.379±0.003
9.0	0.1909	0.380±0.004
10.0	0.1837	0.380±0.004
11.0	0.1772	0.380±0.004
12.0	0.1729	0.380±0.006
13.0	0.1603	0.381±0.003
14.0	0.1535	0.382±0.004
15.0	0.1408	0.383±0.006

In Table I we give the values of f_p and average pressures of the respective systems. First, we can notice from the results in Table I that the value of f_p for the *cg* system is even lower as for the medium dense liquid with $\rho=0.1$ using the effective potential given by Eq. (10) (see the caption of Table II). This indicates that by using the tabulated numerical effective potentials one can better reproduce the structure of the reference all-atom system than by using the analytical potentials. Second, using the linear correction term Eq. (13) one can match the pressures in the *cg* system with the reference value of the all-atom model system.

The equations of state for *ex* and *cg* systems using the tabulated effective potential $U_{tab}^{cm}(r)$ are displayed in Fig. 4. We can see that the equations of state now, as expected, coincide around the phase point at $\rho=0.175$. However, for lower densities the effective potential given by Eq. (10), which is parametrized for $\rho=0.1$, better reproduces the ref-

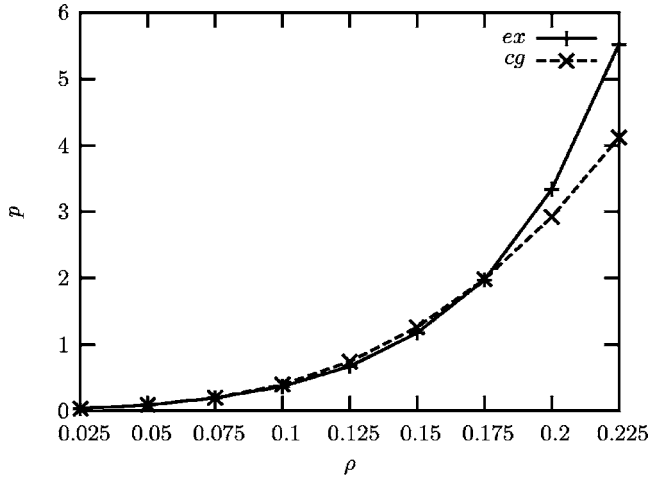

FIG. 4. Equations of state at $T=1$ for the *ex* and *cg* systems using the tabulated effective potential $U_{tab}^{cm}(r)$. Shown is the pressure p as a function of the number density ρ of the system.

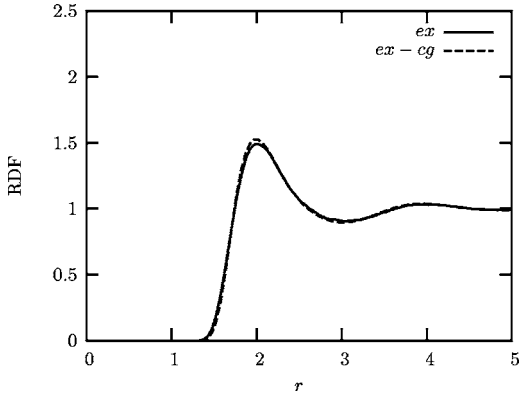

FIG. 5. RDF_{cm}s of the *ex* and *ex-cg* systems with $r_0=12.0$ and $d=2.5$ at $\rho=0.1$ and $T=1$.

erence equation of state [1]. This implies that one should reparametrize the effective pair potential for different phase points considered as already argued in Ref. [1]. Therefore, by the effective pair potential reparametrization we could also extend our methodology to densities higher than $\rho=0.175$.

Using Eq. (11) we also computed the heat capacities per molecule C_V^{ex} and C_V^{cg} for the high density liquid. The corresponding values are $C_V^{ex}=9.5\pm0.5$ and $C_V^{cg}=2.4\pm0.1$, respectively. Their ratio $C_V^{ex}/C_V^{cg}\approx4$ is as in the case of the medium dense liquid close to 4.

B. Hybrid atomistic/mesoscale (*ex-cg*) system

1. Medium dense liquid

To validate the results of AdResS we compare the computed statistical properties of the hybrid *ex-cg* system, as introduced in Sec. III, with the corresponding properties of the *ex* system.

In Fig. 5 we depict RDF_{cm}s of the *ex* and *ex-cg* systems at $\rho=0.1$ and $T=1$. Since the AdResS gives acceptable results for the interface region with widths larger than the maximal range of interaction [1] we set in this study $d=2.5$. Shown is the case where the radius of the all-atom region is $r_0=12.0$. The RDF_{cm} of the *ex-cg* system matches up to a given accuracy of our parametrization to the RDF_{cm} of the reference *ex* system indicating that the AdResS accurately reproduces the structure also in the case of the spherical shaped regions with a different level of detail. This is even more clear from the results given in Table II, where the f_p and average pressure are given as a functions of r_0 for the *ex-cg* system. Clearly, the value of f_p decreases with the growing radius of the all-atom region r_0 demonstrating that the RDF_{cm} of the *ex -cg* system converges towards the reference RDF_{cm} of the *ex* system. This is, of course, the basic condition for the working hybrid scheme since any calculated observable should converge towards the reference value by increasing the size of the all-atom region. Yet, we can see from the results in Table II that this is not the case for the pressure, which is slightly increasing with the growing r_0 in the *ex-cg* system. This is because the size (volume) of the interface region, in which the pressure is overestimated using Eq. (4), is growing as $4\pi[(r_0+d)^3-r_0^3]/3$ with the growing r_0. This is, of course,

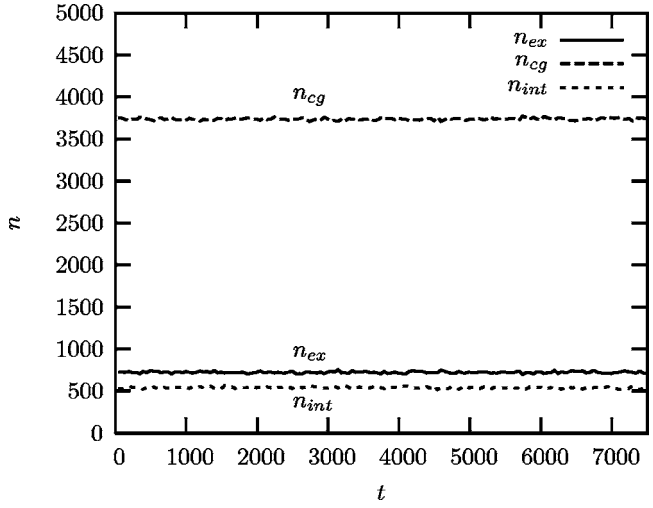

FIG. 6. Time evolution of the number of molecules in the *ex*, *cg*, and interface (*int*) regions of the *ex-cg* system with $r_0=12.0$ and $d=2.5$ at $\rho=0.1$ and $T=1$. The average numbers of molecules in the *ex*, *cg*, and *int* regions are 724 ± 35, 3736 ± 53, and 539 ± 32, respectively.

a finite size effect and should diminish with the growing system size when the size of the transition regime becomes negligible in comparison to the rest of the system.

The structure of the underlying *ex* system is accurately reproduced using the AdResS because the number of molecules in the interface regime is small in comparison to the rest of the system as can be observed from the results in Fig. 6 where the time evolution of number of molecules in all three different regimes of hybrid systems with $r_0=12.0$ and $d=2.5$ is displayed. The theoretical estimates, which are in a good agreement with the simulation averages, for the numbers of molecules in different regions of a homogeneous liquid are $n_{ex}=\rho V_{ex}=723$, $n_{cg}=\rho V_{cg}=3724$, and $n_{int}=\rho V_{int}=553$, where V_{ex}, V_{cg}, and V_{int} are the volume sizes of *ex*, *cg*, and interface (*int*) regions, respectively. The number of molecules in the all-atom and interface domains is much lower than in the *cg* region as will also be the case in the MD simulations of realistic soft matter systems in order to reduce the computational costs. The results in Fig. 6 demonstrate that also for the case of the spherical shape of the atomistic and coarse-grained regimes the AdResS guarantees that the chemical potentials at the boundary between regions with different levels of detail are equal as required by Eq. (8).

This is further supported by the results presented in Fig. 7, in which we present the normalized radial number density profiles of the *ex-cg* system with $r_0=6.0$ and $r_0=12.0$. One can observe that the density in the *ex* and *cg* regimes of the *ex-cg* system is equal to the reference density $\rho_0=0.1$. As in the example of flat boundary between different regimes [1], the density oscillates around the reference value with an amplitude of approximately 0.05ρ in the interface region of the *ex-cg* system.

2. High density liquid

Using the $U_{tab}^{cm}(r)$ for defining the effective pair interactions in the system we have computed as in the case of a

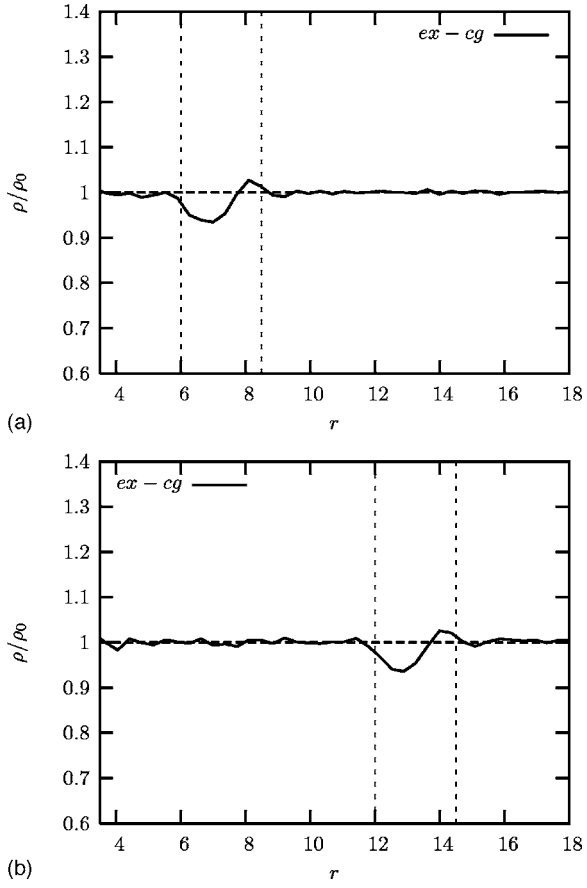

FIG. 7. The normalized radial number density profiles of the *ex-cg* system at $\rho=0.1$ and $T=1$. (a) $r_0=6.0$. (b) $r_0=12.0$. The vertical lines denote the boundaries of the interface region with $d=2.5$.

medium dense liquid with $\rho=0.1$ the RDF$_{cm}$s, f_p, average pressure, time evolution of number of molecules in the different regimes in the system, and the density profiles of the *ex-cg* system at $\rho=0.175$ and $T=1$, as presented in Fig. 8, Table III, and Figs. 9 and 10, respectively. Although the range of the effective pair interactions is here 3.5, as one can observe from the curves in Fig. 3(a) the interactions are so

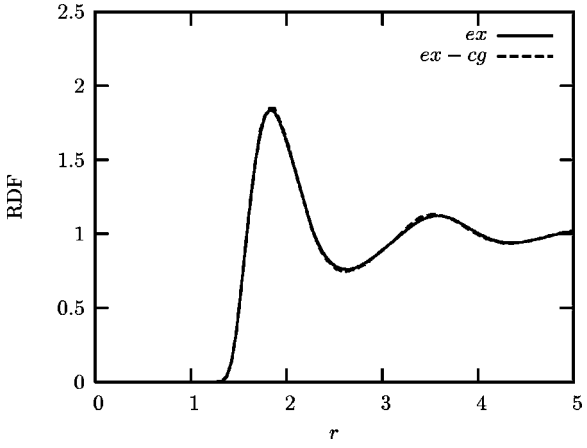

FIG. 8. RDF$_{cm}$s of the *ex* and *ex-cg*, and systems with $r_0=6.0$ and $d=2.5$ at $\rho=0.175$ and $T=1$.

TABLE III. Penalty function f_p defined by Eq. (14) and average pressure p for the *ex-cg* system at $\rho=0.175$ and $T=1$ as a function of r_0.

r_0	$f_p\times 10^3$	p
6.0	0.0246	1.99±0.01
7.0	0.0263	1.99±0.02
8.0	0.0273	1.99±0.02
9.0	0.0293	2.00±0.01
10.0	0.0350	2.01±0.02
11.0	0.0400	2.01±0.02
12.0	0.0488	2.02±0.02

small for the distances beyond 2.5 that we set $d=2.5$ also in this case in order to minimize the size of the transition regime.

The conclusions on the basis of results in Fig. 8, Table III, and Fig. 9 are the same as in the case of the medium dense liquid with $\rho=0.1$, i.e., the AdResS accurately reproduces the statistical properties of the reference *ex* system. Actually, the reproduction of the RDF$_{cm}$s of the reference *ex* system is in this case even better due to the usage of the tabulated numerical effective pair potential. Note, however, that here f_p reported in Table III goes up with r_0 in contrast to the case of the medium dense liquid. This is because the amplitude of density variations in the transition regime increases in comparison with the medium dense liquid as it can be observed from the density profile of the *ex-cg* system presented in Figs. 10(a) and 10(b), respectively. The increased density fluctuations slightly affect the quality of the computed RDF$_{cm}$s for this moderate system size. Since the size of the transition regime, as already explained, grows with r_0 the value f_p goes up with r_0. The amplitude of density oscillations in the transition regime increases because the interac-

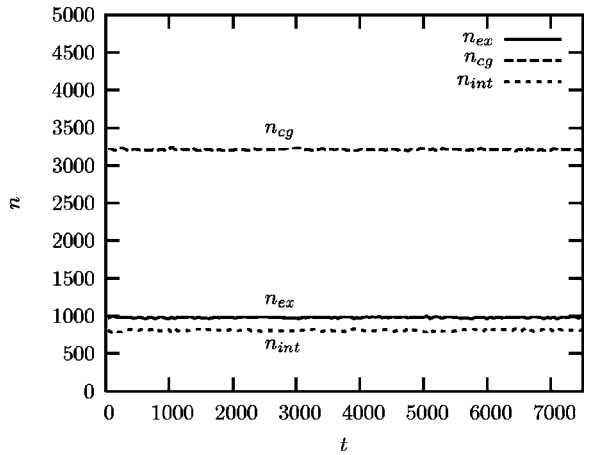

FIG. 9. Time evolution of the number of molecules in different regimes of the *ex-cg* system with $r_0=11.0$ and $d=2.5$ at $\rho=0.175$ and $T=1$. The theoretical predictions for the numbers of molecules in different regions of a homogeneous liquid are $n_{ex}=975$, $n_{cg}=3197$, and $n_{int}=828$. The corresponding simulation averages in the *ex*, *cg*, and interface (*int*) regions are 979±31, 3210±33, and 809±26, respectively.

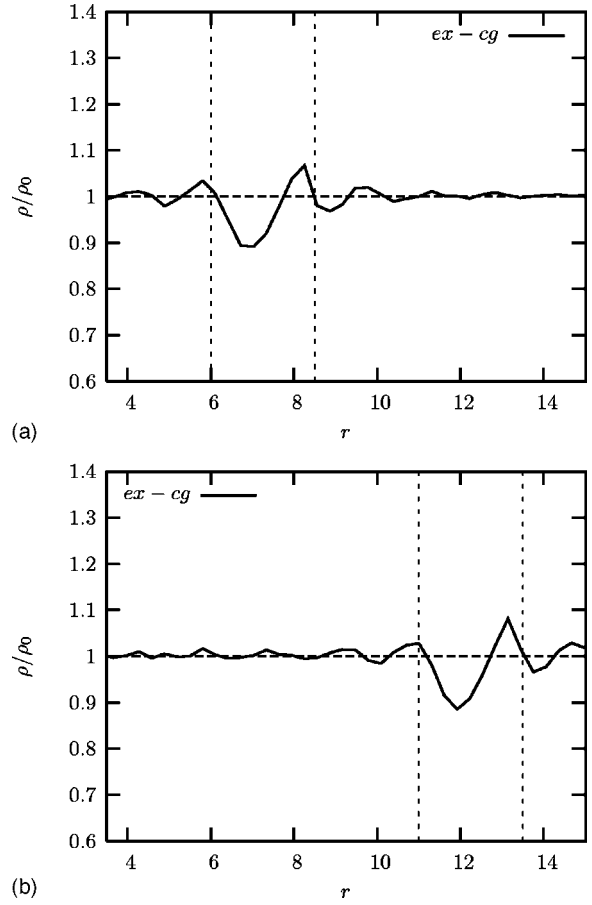

FIG. 10. The normalized radial number density profiles of the *ex-cg* system at $\rho=0.175$ and $T=1$. (a) $r_0=6.0$. (b) $r_0=11.0$. The vertical lines denote the boundaries of the interface region with $d=2.5$.

tions between molecules are stronger in the denser liquid and the artifact of Eq. (4) is more prominent in this case. This can be explained by the fact that a linear combination of two systems, which have the same equations of state, usually does not have the same equation of state as the respective systems. However, using the interface pressure correction presented in the next subsection, we managed to reduce considerably the density and pressure oscillations in the transition regime.

C. Interface pressure correction

Intuitively, a normalized linear combination of explicit and coarse-grained forces given by the ansatz in Eq. (4) that defines the interactions of hybrid molecules in the transition regime should yield an effective interaction that gives a pressure that is close to the respective pressure values in the *ex* and *cg* systems. However, as found in Ref. [1], the pressure in a system containing exclusively the hybrid molecules with the constant $w\neq 0,1$ is slightly dependent on the w value, i.e., the ratio between the explicit-explicit and mesoscoscale-mesoscale interactions. This indicates that each system composed of exclusively the hybrid molecules with a different constant w is due to different effective interactions at a slightly different state point than the *ex* and *cg* systems. This causes the pressure and density variations in the interface layer as evident from Figs. 7 and 10.

Here, we correct for this by a reparametrization of the effective pair potential in the system composed of exclusively hybrid molecules with the constant $w=\frac{1}{2}$ over the whole system. In the definition of intermolecular forces in the hybrid atomistic/mesoscale system, Eq. (4), we then replace the expression for the effective pair force given by Eq. (5) with

$$\mathbf{F}_{\alpha\beta}^{cm}=s[w(R_\alpha)w(R_\beta)]\mathbf{F}_{\alpha\beta_o}^{cm}+(1-s[w(R_\alpha)w(R_\beta)])\mathbf{F}_{\alpha\beta_{ic}}^{cm}, \tag{15}$$

where the function $s\in[0,1]$ is defined as

$$s[x]=4\left(\sqrt{x}-\tfrac{1}{2}\right)^2, \tag{16}$$

so that $s[0]=1$, $s[1]=1$, and $s\left[\frac{1}{4}\right]=0$. The force $\mathbf{F}_{\alpha\beta_o}^{cm}$ is the "original" effective pair force between molecules α and β defined by the effective pair potential, which is obtained by mapping the *cg* model to the *ex* model as explained in Sec. V A. The "interface correction (ic)" force $\mathbf{F}_{\alpha\beta_{ic}}^{cm}$ is the effective pair force between molecules α and β defined by the effective pair potential, which is obtained by mapping the hybrid model system composed of exclusively hybrid molecules with $w=\frac{1}{2}$ to the *ex* model system. The force $\mathbf{F}_{\alpha\beta}^{cm}$ given by Eq. (15) is thus slightly different than $\mathbf{F}_{\alpha\beta_o}^{cm}$ used in the original scheme. The even function given by Eq. (16) is the simplest symmetrical choice to correct the effective pair interactions in the transition regime while leaving the (correct) effective pair interactions in the coarse-grained and atomistic regimes unchanged.

Further improvement could be achieved by additional effective potential derivations obtained by mapping the hybrid systems composed of exclusively the hybrid molecules with different constant values of w to the *ex* system and then use a table for each value of $w(R_\alpha)w(R_\beta)$ for the effective pair interactions calculation. This would soften the resolution switching in a similar way as it is done in the thermodynamic integration [29] for the free energy difference calculations. The price to pay are the additional force calculations of hybrid molecules with the neighboring molecules. Thus, there is the trade-off between the accuracy in the transition regime and computational costs of the method.

1. Medium dense liquid

Similarly as we derived $U^{cm}(r)$ given by Eq. (10) [1] we derive the corrected effective potential $U_{ic}^{cm}(r)$ by mapping $ex\text{-}cg\left(w=\frac{1}{2}\right)_{ic}$ system containing exclusively the hybrid molecules with constant $w=\frac{1}{2}$ to the *ex* system at $\rho=0.1$ and $T=1$. $U_{ic}^{cm}(r)$ which recovers the RDF_{cm} and pressure of the underlying *ex* system is also parametrized with the analytical Morse potential

$$U_{ic}^{cm}(r)=\gamma_{ic}(1-\exp[-\kappa(r-r_c)])^2, \tag{17}$$

with the same parameters as the effective potential given by Eq. (10) except from $\gamma_{ic}=0.045$.

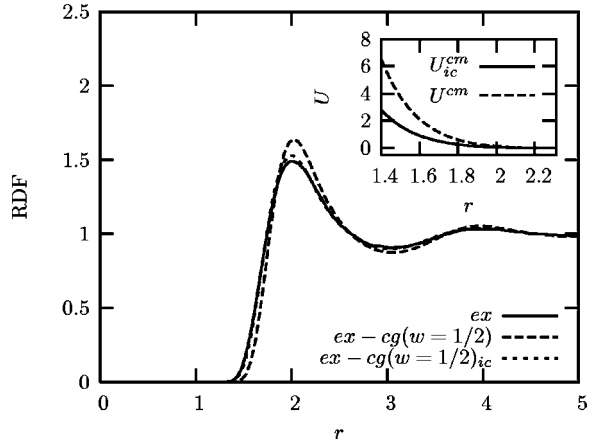

FIG. 11. RDF_{cm}s of the *ex*, *ex-cg*$(w=\frac{1}{2})$, and *ex-cg*$(w=\frac{1}{2})_{ic}$) systems at $\rho=0.1$ and $T=1$. In the inset the corrected effective pair potential $U_{ic}^{cm}(r)$ for hybrid molecules as defined by Eq. (17) and the effective pair potential $U^{cm}(r)$ as defined by Eq. (10) are shown.

The effective potentials given by Eqs. (10) and (17) are depicted in the inset of Fig. 11. The interactions defined by the effective potential $U_{ic}^{cm}(r)$ have the same interaction range as the effective interactions determined by $U^{cm}(r)$, yet they are weaker at short distances. This is to compensate for too strong interactions between molecules in the interface region arising from the normalized linear combination of the atomic and effective pair forces using the ansatz given by Eq. (4).

In Fig. 11 we present RDF_{cm}s of *ex*, *ex-cg*$(w=\frac{1}{2})$, and *ex-cg*$(w=\frac{1}{2})_{ic}$ systems at $\rho=0.1$ and $T=1$. The results demonstrate that by using the effective pair potential given by Eq. (10) for a calculation of the effective pair interactions in the *ex-cg*$(w=\frac{1}{2})$ system, which contains exclusively the hybrid molecules with $w=\frac{1}{2}$, we cannot reproduce satisfactorily the structure of the reference all-atom system. The coordination at the first peak is overestimated in the *ex-cg*$(w=\frac{1}{2})$ system using this potential. In contrast, using the effective potential given by Eq. (17) for a calculation of the effective pair interactions in the *ex-cg*$(w=\frac{1}{2})_{ic}$ system we can again reproduce satisfactorily the structure of the reference all-atom system.

This observations can be further confirmed by the corresponding values of f_p defined by Eq. (14). The values of the f_p for *ex-cg*$(w=\frac{1}{2})$, and *ex-cg*$(w=\frac{1}{2})_{ic}$ systems are given in Table IV. The results clearly demonstrate that using the corrected effective potential from Eq. (17) improves the structure in the *ex-cg*$(w=\frac{1}{2})_{ic}$ system.

In order that the equations of state of the *ex-cg*$(w=\frac{1}{2})_{ic}$ and *ex* systems coincide around the state point at $\rho=0.1$ and $T=1$ the pressures of both systems must also be the same at this phase point. The corresponding pressure values are also reported in Table IV. We can see that the pressure in the *ex-cg*$(w=\frac{1}{2})_{ic}$ system with the applied pressure correction as given by Eq. (15) is much closer to the desired value of the underlying *ex* system than this is the case for the *ex-cg*$(w=\frac{1}{2})$ system without this correction.

TABLE IV. Penalty function f_p defined by Eq. (14) and average pressure p for *ex-cg*$(w=\frac{1}{2})$ and *ex-cg*$(w=\frac{1}{2})_{ic}$ systems at $\rho=0.1$ and $T=1$.

System	$f_p\times10^3$	p
ex-cg$(w=\frac{1}{2})$	2.9284	0.426±0.006
ex-cg$(w=\frac{1}{2})_{ic}$	0.0989	0.375±0.006

TABLE V. Penalty function f_p defined by Eq. (14) and average pressure p for the *ex-cg*$_{ic}$ system at $\rho=0.1$ and $T=1$ as a function of r_0.

r_0	$f_p\times10^3$	p
6.0	0.1923	0.378±0.004
7.0	0.1878	0.378±0.004
8.0	0.1842	0.378±0.001
9.0	0.1731	0.378±0.004
10.0	0.1684	0.378±0.003
11.0	0.1578	0.379±0.005
12.0	0.1464	0.379±0.005
13.0	0.1316	0.379±0.004
14.0	0.1168	0.378±0.005
15.0	0.1051	0.379±0.006

In Table V we give the f_p and average pressure as a functions of r_0 for the *ex-cg*$_{ic}$ system. The latter is the hybrid atomistic/mesoscale system, described in Sec. III, where the interface pressure correction according to Eq. (15) is employed.

The results in Table V demonstrate that the RDF_{cm} of the *ex-cg*$_{ic}$ system match up with the RDF_{cm} of the reference *ex* system. This shows that the AdResS accurately reproduces the structure also with the pressure correction applied. As in the case of the *ex-cg* system with the growing radius of the all-atom region r_0 the values of f_p are decreasing. In contrast to the the *ex-cg* system the pressure also converges with the growing r_0 to the correct value of the reference *ex* system, indicating that the pressure correction given by Eq. (15) successfully removes this artifact of the original scheme already for moderate system sizes.

The average numbers of molecules in the *ex*, *cg*, and interface (*int*) regions of the *ex-cg*$_{ic}$ system with $r_0=12.0$ are 722±25, 3726±41, and 552±24, respectively. These values are in agreement with the corresponding results for the *ex-cg* system with $r_0=12.0$ given in Fig. 6. We demonstrated in Ref. [1] for the flat boundary geometry that molecules can diffuse freely across the interface layer of the *ex-cg* system despite the pressure and density oscillation occuring in that layer. Hence, the agreement between molecular number fluctuations in *ex-cg* and *ex-cg*$_{ic}$ systems indicates that the interface pressure correction given by Eq. (15) does not influence the diffusion across the interface region.

The normalized radial density profile for the *ex-cg*$_{ic}$ system with $r_0=12.0$ at $\rho=0.1$, and $T=1$ is shown in Fig. 12. We can see that the oscillation amplitude is considerably reduced exploiting the pressure correction given by Eq. (15) leading to the correct pressure in the system. Note that we could reduce the density oscillations in the transition regime even

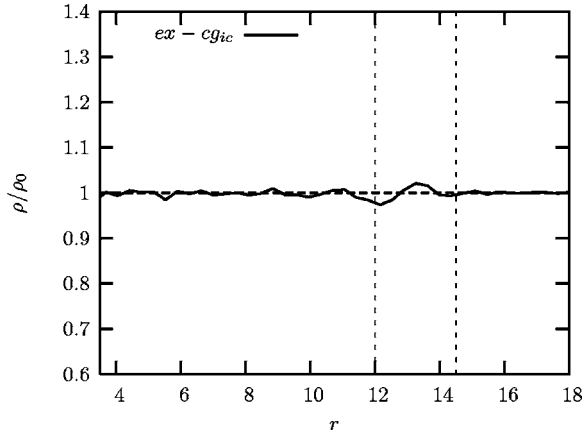

FIG. 12. The normalized radial number density profile of the *ex-cg*$_{ic}$ system with $r_0=12.0$ at $\rho=0.1$ and $T=1$. The vertical lines denote the boundaries of the interface region with $d=2.5$.

further as explained in Sec. V C. This might, in general, not even be necessary since the interface region will represent a minor portion of the system in MD simulations of the realistic soft matter systems.

2. High Density Liquid

We derive the effective pair potential $U^{cm}_{tab_{ic}}(r)$ by mapping the *ex-cg*$\left(w=\frac{1}{2}\right)_{ic}$ system at $\rho=0.175$ and $T=1$ to the corresponding *ex* system using the iterative Boltzmann inversion given by Eqs. (12) and (13) with the same parameters as for the derivation of the tabulated effective potential $U^{cm}_{tab}(r)$ for the *cg* system at $\rho=0.175$ and $T=1$. The effective pair potential defined by Eq. (17) is used as the initial guess for the iteration.

The tabulated numerical effective pair potential $U^{cm}_{tab_{ic}}(r)$ obtained after 5 iterations with $U_0=0.2$ followed by another 4 iterations with $U_0=0.1$ is depicted in the inset of Fig. 13. As for the medium dense liquid $U^{cm}_{tab_{ic}}(r)$ is softer than

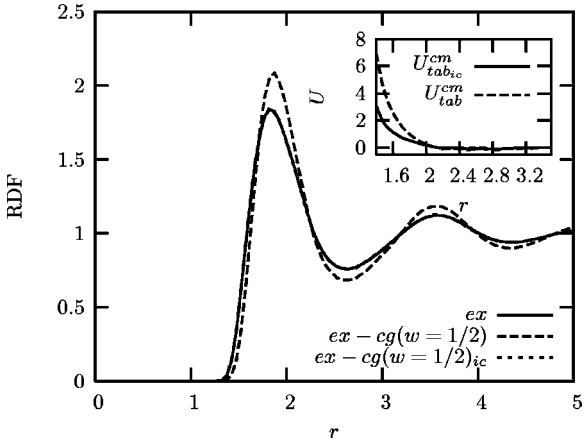

FIG. 13. RDF$_{cm}$s of the *ex*, *ex-cg*$\left(w=\frac{1}{2}\right)$, and *ex-cg*$\left(w=\frac{1}{2}\right)_{ic}$ systems at $\rho=0.175$ and $T=1$. The RDF$_{cm}$s of the *ex* and *ex-cg*$\left(w=\frac{1}{2}\right)_{ic}$ systems match within the line thickness. In the inset the corresponding corrected effective pair potential $U^{cm}_{tab_{ic}}(r)$ and the effective pair potential $U^{cm}_{tab}(r)$ are shown.

TABLE VI. Penalty function f_p defined by Eq. (14) and average pressure p for *ex-cg*$\left(w=\frac{1}{2}\right)$ and *ex-cg*$\left(w=\frac{1}{2}\right)_{ic}$ systems at $\rho=0.175$ and $T=1$.

System	$f_p\times10^3$	p
ex-cg$\left(w=\frac{1}{2}\right)$	5.5716	2.51±0.02
ex-cg$\left(w=\frac{1}{2}\right)_{ic}$	0.0137	1.98±0.02

$U^{cm}_{tab}(r)$. The RDF$_{cm}$s of the *ex*, *ex-cg*$\left(w=\frac{1}{2}\right)$, and *ex-cg*$\left(w=\frac{1}{2}\right)_{ic}$ are shown in Fig. 13.

Similarly to the system with $\rho=0.1$ the agreement for the *ex-cg*$\left(w=\frac{1}{2}\right)$ system, in which $U^{cm}_{tab}(r)$ is used to define the effective interactions between molecules, is worse. These observations are in agreement with the results given in Table VI, where we give f_p and average pressures of the respective systems. The pressure in the *ex-cg*$\left(w=\frac{1}{2}\right)$ system is as in the case of the system with $\rho=0.1$ overestimated. However, we can correct for this artifact using the interface pressure correction according to Eq. (15) and $U^{cm}_{tab_{ic}}(r)$ for computing the interactions in the *ex-cg*$\left(w=\frac{1}{2}\right)_{ic}$ system.

The f_p and the average pressure of the *ex-cg*$_{ic}$ system at $\rho=0.175$ and $T=1$ are given in Table VII.

From the results presented in Table VII we can see that the value of f_p decreases with the growing r_0 while the average pressure corresponds to the value in the reference all-atom system. The statistical properties of the hybrid system employing the interface pressure correction given by Eq. (15) thus converge to the corresponding properties of the all-atom system by increasing the size of the all-atom regime as demanded from a working hybrid scheme.

Also for the high density liquid the average numbers of molecules in the *ex*, *cg*, and interface (*int*) regions of the *ex-cg*$_{ic}$ system with $r_0=11.0$, which are 976±20, 3199±63, and 823±21, respectively, are in good agreement with the corresponding numbers of the *ex-cg* system. In addition, we also computed the fluctuations and average numbers of molecules in the sphere with the center positioned in one of the corners of the simulation box. The corresponding values for the *ex-cg* system are 982±13, 3184±62, and 832±26 for the molecules with the radial distance r from the corner of the simulation box such that $r_0>r\geq0$, $r\geq r_0+d$, and $r_0+d>r\geq r_0$, respectively. The same values for the *ex-cg*$_{ic}$

TABLE VII. Penalty function f_p defined by Eq. (14) and average pressure p for the *ex-cg*$_{ic}$ system at $\rho=0.175$ and $T=1$ as a function of r_0.

r_0	$f_p\times10^3$	p
6.0	0.0228	1.98±0.02
7.0	0.0230	1.98±0.02
8.0	0.0211	1.98±0.02
9.0	0.0198	1.98±0.01
10.0	0.0189	1.98±0.02
11.0	0.0165	1.98±0.02
12.0	0.0132	1.98±0.01

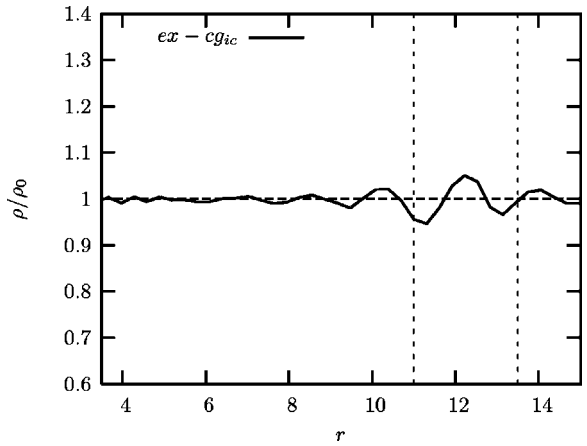

FIG. 14. The normalized radial number density profile of the *ex-cg*$_{ic}$ system with $r_0=11.0$ at $\rho=0.175$ and $T=1$. The vertical lines denote the boundaries of the interface region with $d=2.5$.

system are 976±25, 3194±69, and 827±42, respectively. Because these values are in agreement with the corresponding values n_{ex}, n_{cg}, and n_{int} for the sphere positioned in the center of the simulation box, this indicates that there is no net flux of molecules in the system. Hence, the interface pressure correction given by Eq. (15) has a negligible effect on the diffusion of molecules across the interface layer also for the high density liquid. Furthermore, this also shows that the increased density and pressure fluctuations in the transition regime of the high density *ex-cg* system do not affect significantly the diffusion of molecules across the interface, so that the molecules can freely move across between the all-atom and mesoscale regimes.

Finally, in Fig. 14 we present the normalized radial density profile for the *ex-cg*$_{ic}$ system with $r_0=11.0$ at $\rho=0.175$ and $T=1$. By comparing the density profile in Fig. 14 with its counterpart for the *ex-cg* system shown in Fig. 10 we can conclude that by using the interface pressure correction given by Eq. (15) we can considerably reduce the density oscillations also in the case of the high density liquid. This demonstrates the reliability of our approach.

VI. CONCLUSIONS

In this work we have extended the applicability of the adaptive resolution MD scheme (AdResS) introduced in Ref. [1], that allows us to switch the level of detail on-the-fly during the course of a MD simulation, to the case of the spherical geometry where the atomistic region is in the center of the simulation box surrounded by the mesoscopic region. This situation is appropriate for simulations of biological macromolecules embedded in a solvent. As a model system we have employed a liquid of tetrahedral molecules, which we had introduced in Ref. [1]. Next, we have managed to reduce the pressure and density variations that occurred at the interface region between the atomistic and mesoscopic regimes as an artifact of the original method. We achieve that by reparametrizing the effective pair potential for interactions of the hybrid molecules in the interface region. Finally, we have also tested the new method on a high density liquid with the density corresponding to the high density Lennard-Jones liquid. In contrast to the study presented in Ref. [1] we have here resorted to the tabulated numerical effective potentials that are able to reproduce the structure of the reference all-atom system with the higher accuracy than the analytical counterparts. The simulation results indicate that the AdResS accurately reproduces the statistical properties of the reference all-atom system regardless of the geometry of the regions with different levels of detail and regardless of the density considered. In principle, one could derive the full density dependency of the effective potential to cover the whole density range but this was not in the focus here. Our method, which enables us to cover much longer length scales than the conventional all-atom MD simulation, can also be combined with the hybrid atomistic-continuum MD simulation methods for fluids, see, e.g., Refs. [30–34], to bridge over an even larger range of length scales in such systems. Our long term aim is to extend this methodology from molecular liquids to macromolecular systems in a solution or melt, and liquid crystaline systems.

ACKNOWLEDGMENTS

We are grateful to P. Schravendijk, A. Arnold, M. Deserno, and N. van der Vegt for fruitful discussions. This work was supported in part by the Volkswagen foundation. One of the authors (M. P.) acknowledges the support of the Ministry of Higher Education, Science and Technology of Slovenia under Grant No. P1-0002.

[1] M. Praprotnik, L. Delle Site, and K. Kremer, J. Chem. Phys. **123**, 224106 (2005).
[2] L. Delle Site, C. F. Abrams, A. Alavi, and K. Kremer, Phys. Rev. Lett. **89**, 156103 (2002).
[3] C. F. Abrams, L. Delle Site, and K. Kremer, Phys. Rev. E **67**, 021807 (2003).
[4] L. Delle Site, S. Leon, and K. Kremer, J. Am. Chem. Soc. **126**, 2944 (2004).
[5] E. Villa, A. Balaeff, L. Mahadevan, and K. Schulten, Multiscale Model. Simul. **2**, 527 (2004).
[6] M. Neri, C. Anselmi, M. Cascella, A. Maritan, and P. Carloni, Phys. Rev. Lett. **95**, 218102 (2005).
[7] C. F. Abrams, J. Chem. Phys. **123**, 234101 (2005).
[8] P. Schravendijk, N. van der Vegt, L. Delle Site, and K. Kremer, ChemPhysChem **6**, 1866 (2005).
[9] S. O. Nielsen, G. Srinivas, and M. L. Klein, J. Chem. Phys. **123**, 124907 (2005).
[10] F. Müller-Plathe, ChemPhysChem **3**, 754 (2002).
[11] R. L. Henderson, Phys. Lett. **49A**, 197 (1974).
[12] D. Reith, M. Pütz, and F. Müller-Plathe, J. Comput. Chem. **24**,

1624 (2003).
[13] A. P. Lyubartsev and A. Laaksonen, Phys. Rev. E **52**, 3730 (1995).
[14] S. Izvekov and G. A. Voth, J. Chem. Phys. **123**, 134105 (2005).
[15] M. Praprotnik and D. Janežič, Journal of Chemical Information and Modeling **45**, 1571 (2005).
[16] D. Janežič, M. Praprotnik, and F. Merzel, J. Chem. Phys. **122**, 174101 (2005).
[17] M. Praprotnik and D. Janežič, J. Chem. Phys. **122**, 174102 (2005).
[18] M. Praprotnik and D. Janežič, J. Chem. Phys. **122**, 174103 (2005).
[19] M. Praprotnik, D. Janežič, and J. Mavri, J. Phys. Chem. A **108**, 11056 (2004).
[20] This is achieved by introducing a slab with the width of the effective interaction range, which continues from the transition into the explicit regime, containing hybrid molecules with $w=1$. These hybrid molecules interact among themselves and also with the explicitly resolved molecules as purely all-atom molecules while each of them still has a center-of-mass interaction site for the interactions with the hybrid molecules with $0<w<1$ in the interface layer. Since the hybrid molecules with $w=1$ have fully equilibrated rotational and vibrational degrees of freedom and the proper orientation in space, we count the respective slab to the explicit rather than to the transition regime.
[21] http://www.espresso.mpg.de.
[22] B. A. Mann, R. Everaers, C. Holm, and K. Kremer, Europhys. Lett. **67**, 786 (2004).
[23] B. Dünweg and W. Paul, Int. J. Mod. Phys. C **2**, 817 (1991).
[24] M. P. Allen and D. J. Tildesley, *Computer Simulation of Liquids* (Clarendon Press, Oxford, 1987).
[25] H. Berendsen, J. Postma, W. van Gunsteren, A. D. Nola, and J. Haak, J. Chem. Phys. **81**, 3684 (1984).
[26] R. L. C. Akkermans and G. Ciccotti, J. Phys. Chem. B **108**, 6866 (2004).
[27] A. A. Louis, J. Phys.: Condens. Matter **14**, 9187 (2002).
[28] G. Milano and F. Müller-Plathe, J. Phys. Chem. B **109**, 18609 (2005).
[29] A. R. Leach, *Molecular Modelling*, 2nd ed. (Pearson Education Limited, Harlow, 2001).
[30] S. T. O'Connell and P. A. Thompson, Phys. Rev. E **52**, R5792 (1995).
[31] N. G. Hadjiconstantinou, Phys. Rev. E **59**, 2475 (1999).
[32] J. Li, D. Liao, and S. Yip, Phys. Rev. E **57**, 7259 (1998).
[33] E. G. Flekkoy, G. Wagner, and J. Feder, Europhys. Lett. **52**, 271 (2000).
[34] R. Delgado-Buscalioni and P. V. Coveney, Phys. Rev. E **67**, 046704 (2003).